Supporting Information

Optimized Ru Catalysts for the Selective Cleavage of C_{Ar}-OCH_3 Bonds in Guaiacol Under Mild Conditions

Chuqiao Song[1], Wei Cheng[1], Xiaojie Wu[1], Shufang Zhao[1,2], Ying Tang[1], Xin Tang[1], Yao Xu[3], Lili Lin[1,2*], Siyu Yao[4*]*

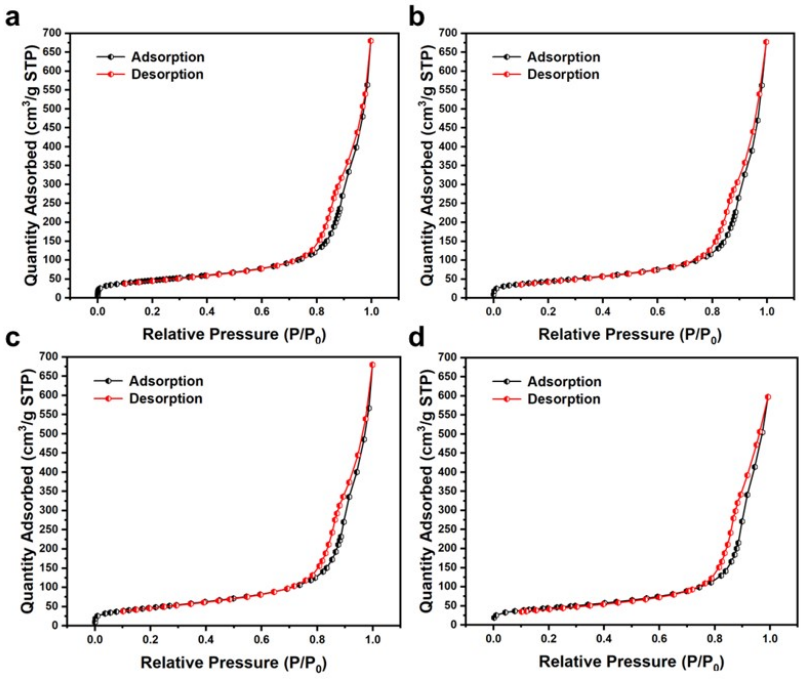

Fig. S1 N_2 adsorption-desorption isotherms of Ru/γ-Al_2O_3 catalysts with different Ru particle sizes. a. $Ru_{0.6}$/γ-Al_2O_3, b. $Ru_{1.5}$/γ-Al_2O_3, c. $Ru_{2.5}$/γ-Al_2O_3, d. $Ru_{7.5}$/γ-Al_2O_3 catalysts.

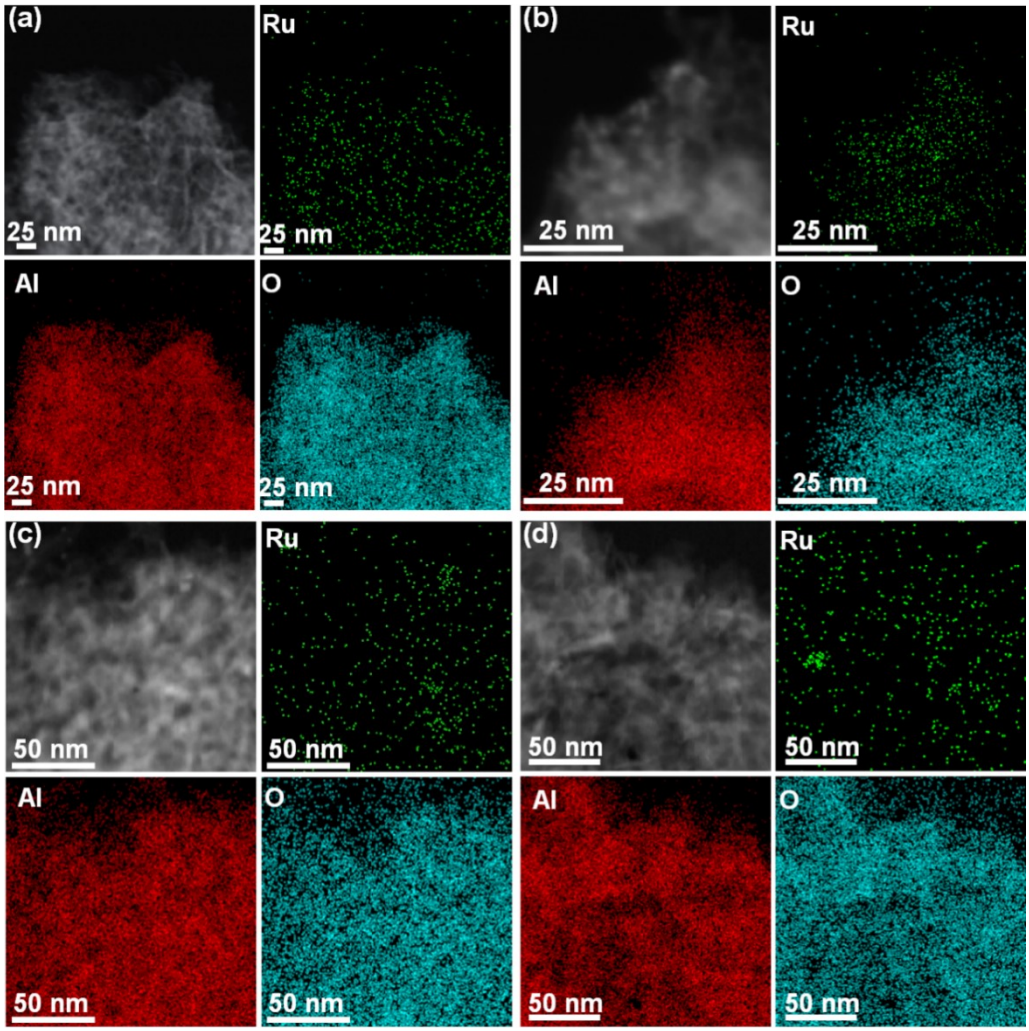

Fig. S2 STEM images and elemental mappings of Ru/γ-Al_2O_3 catalysts with different Ru particle sizes. a. $Ru_{0.6}$/γ-Al_2O_3, b. $Ru_{1.5}$/γ-Al_2O_3, c. $Ru_{2.5}$/γ-Al_2O_3, d. $Ru_{7.5}$/γ-Al_2O_3 catalysts.

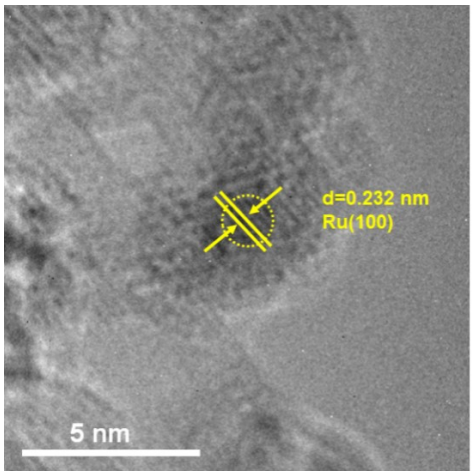

Fig. S3 High-resolution TEM image of the $Ru_{1.5}/\gamma\text{-}Al_2O_3$ catalyst.

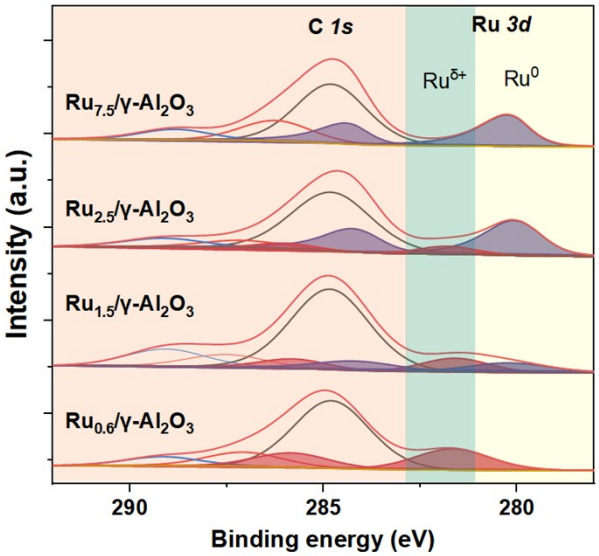

Fig. S4 Quasi-in-situ XPS of $Ru/\gamma\text{-}Al_2O_3$ catalysts. All catalysts are pre-reduced at 200 °C for 2 h.

Table S1. CO-DRIFTS peak assignments and occupied proportion based on fitting results on Ru/γ-Al_2O_3 catalysts.

Catalyst	Frequency (cm^{-1})	Assign	Proportion (%)
$Ru_{0.6}/\gamma$-Al_2O_3	2122	$Ru^{\delta+}$-CO	12.9
	2081	Ru-$(CO)_x$	78.2
	2022	Ru-CO	8.9
$Ru_{1.5}/\gamma$-Al_2O_3	2124	$Ru^{\delta+}$-CO	12.2
	2072	Ru-$(CO)_x$	68.3
	2002	Ru-CO	19.5
$Ru_{2.5}/\gamma$-Al_2O_3	2128	$Ru^{\delta+}$-CO	14.3
	2065	Ru-$(CO)_x$	56.2
	2025，2002	Ru-CO	29.5
$Ru_{7.5}/\gamma$-Al_2O_3	2128	$Ru^{\delta+}$-CO	3.1
	2068	Ru-$(CO)_x$	14.5
	2044，1992	Ru-CO	82.4

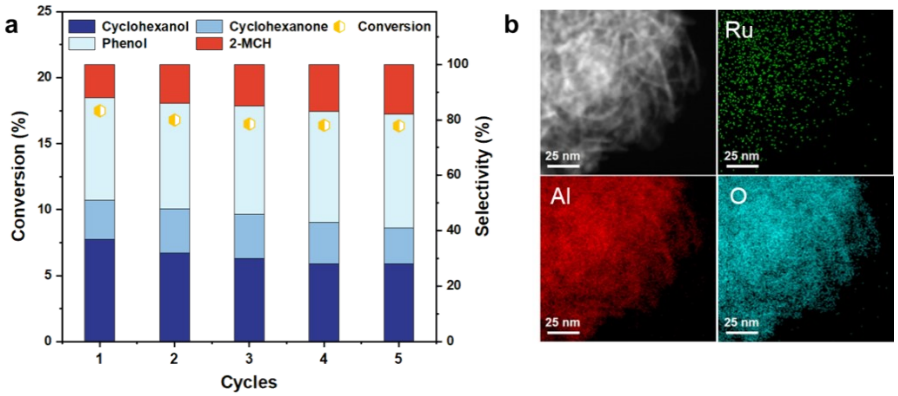

Fig. S5 a. Cycling stability test under low conversion of the $Ru_{1.5}/\gamma\text{-}Al_2O_3$ catalyst at 190 °C for guaiacol hydrodeoxygenation reaction (Reaction condition: 0.3 mmol guaiacol, 0.01 g catalyst, 3.0 mL H_2O, 5 bar H_2, 190 °C, 1/6 h, 400 rpm); b. STEM images and elemental mappings of the used-$Ru_{1.5}/\gamma\text{-}Al_2O_3$ catalyst.

Table S2. Physicochemical properties of the $Ru_{1.5}/\gamma\text{-}Al_2O_3$ catalysts.

Catalyst	**Ru[a] (wt %)**	**S_{BET} (m^2/g)**
$Ru_{1.5}/\gamma\text{-}Al_2O_3$-Fresh	1.50	159.1
$Ru_{1.5}/\gamma\text{-}Al_2O_3$-Used[b]	1.48	112.8

[a]Measured by inductive coupled plasma-optical emission spectroscopy (ICP-OES) on a Varian ICP-OES 720.

[b]The used catalyst was obtained by centrifugation from the solvent, washed several times with deionized water, and dried overnight in an oven at 60 °C before characterizations.

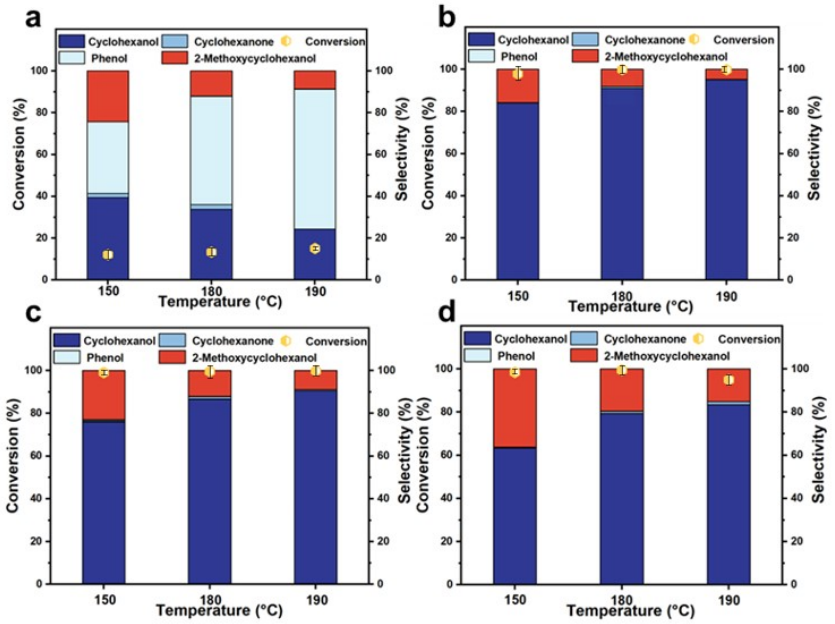

Fig. S6 Catalytic performance of guaiacol hydrodeoxygenation at different temperatures on a. $Ru_{0.6}/\gamma\text{-}Al_2O_3$, b. $Ru_{1.5}/\gamma\text{-}Al_2O_3$, c. $Ru_{2.5}/\gamma\text{-}Al_2O_3$, d. $Ru_{7.5}/\gamma\text{-}Al_2O_3$ catalysts (Reaction condition: 0.3 mmol guaiacol, 0.02 g catalyst, 3.0 mL H_2O, 5 bar H_2, 6 h, 400 rpm, the error bars show the deviation of guaiacol conversion based on three repeated experiments).

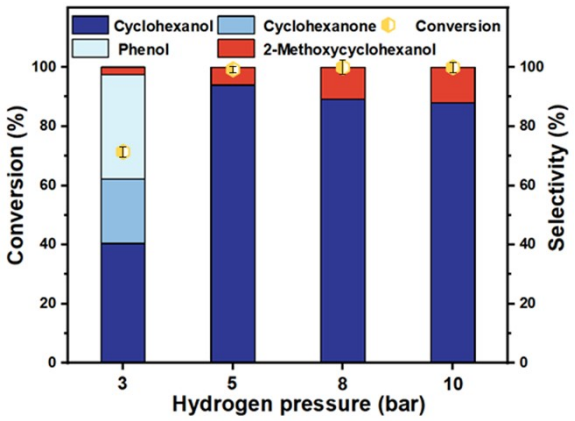

Fig. S7 Catalytic performance of guaiacol hydrodeoxygenation under different H_2 pressure on the $Ru_{1.5}/\gamma\text{-}Al_2O_3$ catalyst (Reaction condition: 0.3 mmol guaiacol, 0.02 g catalyst, 3.0 mL H_2O, 190 °C, 6 h, 400 rpm, the error bars show the deviation of guaiacol conversion based on three repeated experiments).

Table S3. State-of-the-art Ru-based catalysts for hydrodeoxygenation of guaiacol to cyclohexanol

Entry	Catalyst	Reaction condition			Solvent	Conv. /%	Cyclohexanol yield /%	Ref.
		T /°C	$P(H_2)$ /MPa	t /h				
1	**Ru/Al_2O_3**	**190**	**0.5**	**6**	**H_2O**	**99.9**	**95.0**	**This work**
2	Ru/TiO_2	240	1.0	1	dioxane	71.7	51.0	[1]
3	Ru/C	200	-	5	isopropanol	99.0	70.0	[2]
4	Ru-MnO/CNTs	200	2.0	3.33	decahydronaphthalene	99.4	85.8	[3]
5	$2Ru2.5Fe/Al_2O_3$	240	3.0	4	n-octane	99.9	81.3	[4]
6	Ru_1/CeO_2	200	1.0	6	H_2O	99.9	99.9	[5]
7	$RuMn/Al_2O_3$-SiO_2	180	2.0	4	H_2O	100.0	96.8	[6]
8	$Ru/MgO-ZrO_2$	250	1.0	1.5	H_2O	100.0	83.1	[7]
9	Ru/TiO_2-eSiO_2	160	1.5	1.67	H_2O	100.0	84.2	[8]
10	Ru/ZnAlPWO	250	2.0	1	H_2O	100.0	90.0	[9]
11	Ru-MnO_x/C	160	1.5	4	H_2O	100.0	81.0	[10]
12	Ru/C+MgO	160	1.5	2	H_2O	98.0	79.0	[11]
13	Ru/Al_2O_3	225	1.0	4	cyclohexane	100.0	82.0	[12]
14	Ru/Al_2O_3	225	0	2	isopropanol	100.0	74.0	[13]
15	Ru/C	140	3.0	4	CH_3COOH	84.0	63.0	[14]
16	Ru-PAF-30	250	3.0	1	H_2O	100.0	64.0	[15]
17	$HRO/Mg(OH)_2$	160	1.0	6	H_2O	100.0	89.0	[16]

18	5Ru-5Co/TiO_2-Al_2O_3	200	2.0	3.5	decahydronaphthalene	>99	94.0	[17]

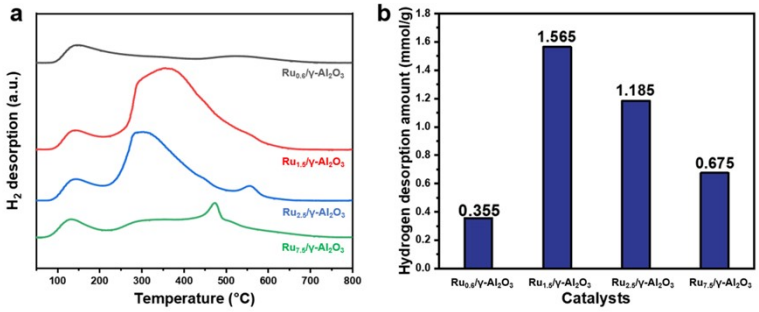

Fig. S8 a. H_2-TPD results; and b. the corresponding H_2 adsorption capacity of Ru/γ-Al_2O_3 catalysts.

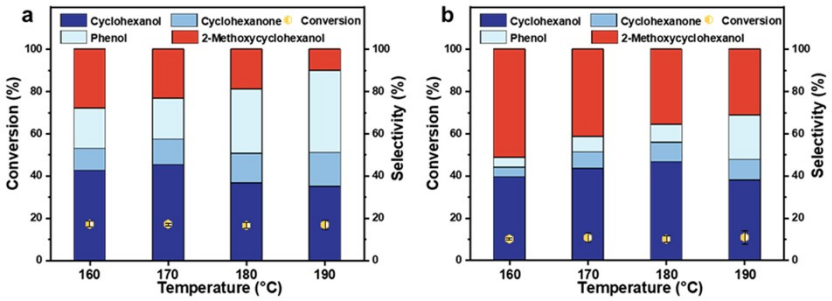

Fig. S9 Catalytic performances of a. the $Ru_{1.5}$/γ-Al_2O_3 and b. the $Ru_{7.5}$/γ-Al_2O_3 at low conversion level of ~15 % at different temperatures. (Reaction condition: 0.3 mmol guaiacol, 0.01 g catalyst, 3.0 mL H_2O, 5 bar H_2, 1/6 h, 400 rpm, the error bars show the deviation of guaiacol conversion based on three repeated experiments).

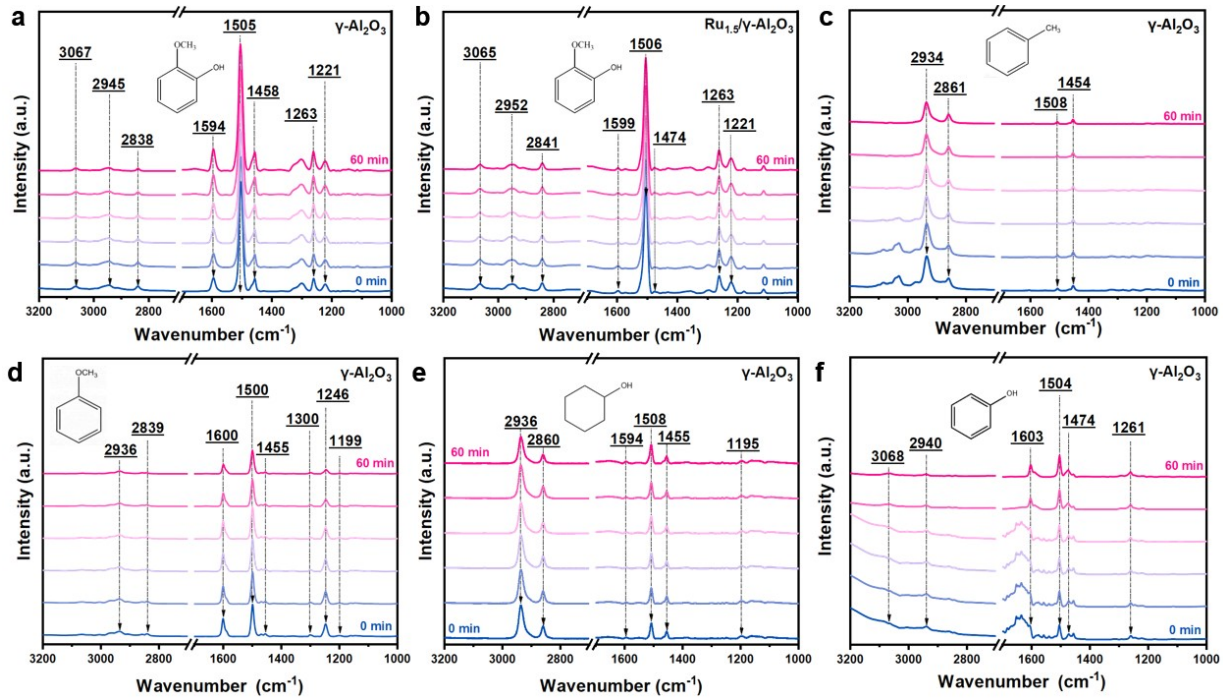

Fig. S10 In situ DRIFTS of adsorption with a. guaiacol on γ-Al_2O_3, b. guaiacol on $Ru_{1.5}$/γ-Al_2O_3, c. methylbenzene on γ-Al_2O_3, d. anisole on γ-Al_2O_3, e. cyclohexanol on γ-Al_2O_3, and f. phenol aqueous solution on γ-Al_2O_3, at 50 ℃.

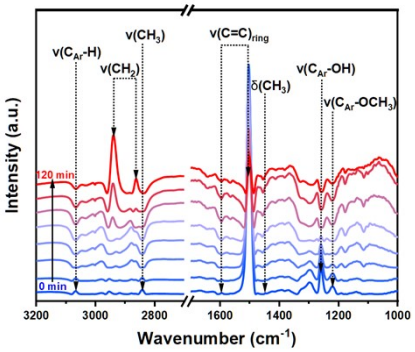

Fig. S11 In situ DRIFTS of the adsorbed intermediate hydrogenation on $Ru_{1.5}/\gamma\text{-}Al_2O_3$ catalyst at 150 ℃ with the inlet gas switched from Ar to 20% H_2 for 120 min.

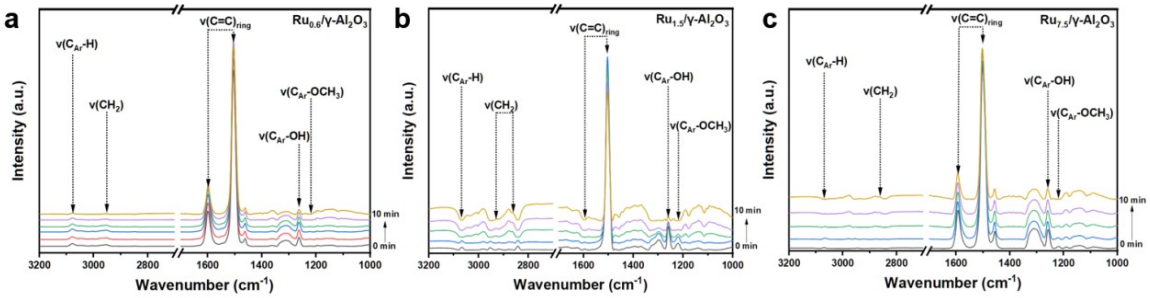

Fig. S12 In situ DRIFTS of the adsorbed intermediate hydrogenation on a. $Ru_{0.6}/\gamma\text{-}Al_2O_3$, b. $Ru_{1.5}/\gamma\text{-}Al_2O_3$ and c. $Ru_{7.5}/\gamma\text{-}Al_2O_3$ catalysts at 150 ℃ with the inlet gas switched from Ar to 20% H_2 for 10 min.

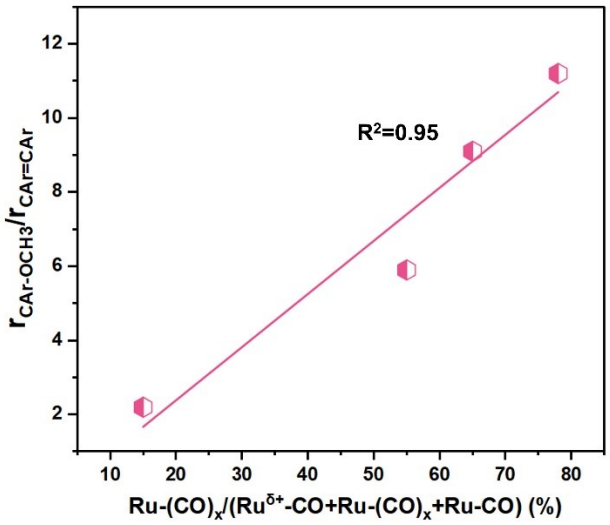

Fig. S13 The relationship between the proportion of low coordinated Ru sites and the relative ratio of $r_{CAr\text{-}OCH3}/r_{CAr=CAr}$ of guaiacol.

Table S4. Formulas to calculate the atom numbers at different sites for each Ru particle [18]

Different sites	Formulas[a]
Total atom number of each particle (N_T[b])	$0.25(14m^3-21m^2+14m-4)$
Surface atom number of each particle (N_s)	$7.5m^2-14m+6$
Corner atom number of each particle (N_{corner})	12
Edge atom number of each particle (N_{edge})	18m-40
Terrace atom number of each particle ($N_{Terrace}$)	$7.5m^2-32m+34$

[a] m is the number of atoms lying on an equivalent edge (corner atoms included).

[b] the particle size with the N_T in one truncated bipyramid follows the relationship of $1.105xN_T^{1/3}xd_{Ru\ atom}$ ($d_{Ru\ atom}$=0.268 nm).

For the fraction of each typed active site per mole of Ru: $y_i=N_i/N_T$.

Given the used mole of Ru in each reaction was kept the same ($n_{Ru}=0.002/M_{Ru}$), the particle numbers of each type active site per mole of Ru were also calculated:

$N_p=n_{Ru}\cdot N_A/N_T=(0.002/M_{Ru})\cdot N_A/N_T$, N_A is the Avogadro constant and M_{Ru} is the molecular weight.

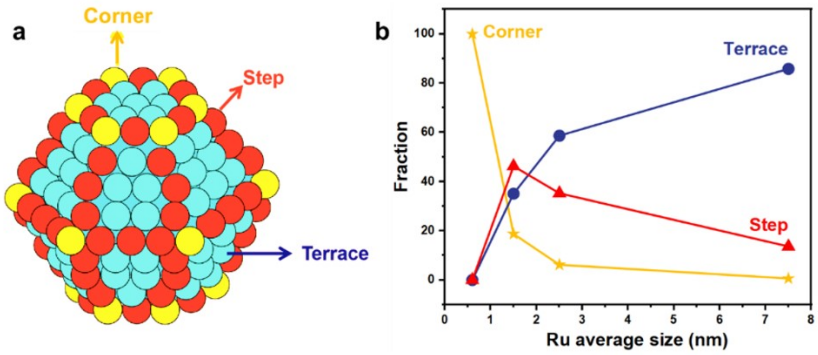

Fig. S14 a. Truncated hexagonal bipyramid structure model; **b.** The proportion of different surface sites obtained from theoretical proportion based on Fig. S14a as a function of Ru particle size.

References

1. X. Wang, P. Wu, Z. Wang, L. Zhou, Y. Liu, H. Cheng, M. Arai, C. Zhang and F. Zhao, *ACS Sustainable Chem. Eng.*, 2021, 9, 3083-3094.

2. M. Kim, J.-M. Ha, K.-Y. Lee and J. Jae, *Catal Commun.*, 2016, 86, 113-118.

3. W. Long, P. Liu, W. Xiong, F. Hao and H. a. Luo, *Can. J. Chem.*, 2019, 98, 57-65.

4. T. Liu, Z. Tian, W. Zhang, B. Luo, L. Lei, C. Wang, J. Liu, R. Shu and Y. Chen, *Fuel*, 2023, 339, 126916.

5. K. Zhang, Q. Meng, H. Wu, J. Yan, X. Mei, P. An, L. Zheng, J. Zhang, M. He and B. Han, *J. Am. Chem. Soc.* 2022, 144, 20834-20846.

6. M. Chen, Q. Zhong, M. Zhang, H. Huang, Y. Liu and Z. Wei, *Catal Commun.*, 2022, 172, 106550.

7. M. Zhang, L. Xiang, G. Fan, L. Yang and F. Li, *Mol. Catal.*, 2022, 533, 112794.

8. B. Han, Z. Bao, T. Liu, H. Zhou, G. Zhuang, X. Zhong, S. Deng and J. Wang, *ChemistrySelect*, 2017, 2, 9599-9606.

9. Z. Wang, A. Wang, L. Yang, G. Fan and F. Li, *Mol. Catal.*, 2022, 528, 112503.

10. M. Ishikawa, M. Tamura, Y. Nakagawa and K. Tomishige, *Appl Catal B-Environ.*, 2016, 182, 193-203.

11. Y. Nakagawa, M. Ishikawa, M. Tamura and K. Tomishige, *Green Chem.*, 2014, 16, 2197-2203.

12. D. Singh and P. L. Dhepe, *Mol. Catal.*, 2020, 480, 110525.

13. T. S. Khan, D. Singh, P. P. Samal, S. Krishnamurty and P. L. Dhepe, *ACS Sustainable Chem. Eng.*, 2021, 9, 14040-14050.

14. C. E. J. J. Vriamont, T. Chen, C. Romain, P. Corbett, P. Manageracharath, J. Peet, C. M. Conifer, J. P. Hallett and G. J. P. Britovsek, *ACS Catal.*, 2019, 9, 2345-2354.

15. L. A. Kulikov, M. A. Bazhenova, D. A. Makeeva, M. V. Terenina, A. L. Maximov and E. A. Karakhanov, *Petroleum Chemistry*, 2022, 62, 1096-1106.

16. S. Gundekari, B. Biswas, T. Bhaskar and K. Srinivasan, *Biomass Bioenergy*, 2022, 161,

106448.

17. W. Zhao, Z. Zhang, B. Wang, Y. Lv, L. Huang and P. Liu, *Appl. Catal., A*, 2024, 678, 119711.

18. M. Ye, Y. Li, Z. Yang, C. Yao, W. Sun, X. Zhang, W. Chen, G. Qian, X. Duan, Y. Cao, L. Li, X. Zhou and J. Zhang, *Angew. Chem. Int. Ed.*, 2023, 62, e202301024.